Process Synthesis for Cascade Refrigeration System Based on Exergy Analysis

Ha Dinh, Jian Zhang, and Qiang Xu
Dan F. Smith Dept. of Chemical Engineering, Lamar University, Beaumont, TX 77710

DOI 10.1002/aic.14843
Published online May 5, 2015 in Wiley Online Library (wileyonlinelibrary.com)

Refrigeration system holds an important role in chemical/petrochemical processes. The traditional cascade refrigeration system (CRS) used in ethylene plants contains multiple refrigerants working at multiple temperature/pressure levels. In this study, a general methodology is developed for the optimal process synthesis of a CRS based on exergy analysis. This procedure involves four stages: (1) refrigeration system exergetic analysis; (2) optimization model development for simultaneous synthesis of refrigeration system and heat exchanger network (HEN); (3) HEN configuration; and (4) final solution validation. The exergy–temperature chart is used to comprehensively analyze a CRS. A mathematical model is presented to minimize total compressor shaft work of the HEN-considered CRS, where multiple recycling loops satisfying all cooling/heating demands are simultaneously addressed. The optimal solution is examined by rigorous simulations to verify its feasibility and consistency. The efficacy of the developed methodology is demonstrated by a case study of a propylene CRS in an ethylene plant. © 2015 American Institute of Chemical Engineers *AIChE J*, 61: 2471–2488, 2015
Keywords: exergy analysis, simulation, optimization, process synthesis, refrigeration system

Introduction

Refrigeration system holds an important role in many chemical/petrochemical processes. In general, it works by employing refrigerant(s) to take heats from low-temperature sources and deliver them to high-temperature sinks at the cost of compression work. Vapor-compression refrigeration systems have been widely used in the chemical process industry (CPI) due to their capacities to cover cooling/heating demands within an adequate range of targeted temperatures. Because refrigeration systems can cool a process system far below the ambient temperature, it is quite indispensable in many large-scale cryogenic separation processes, such as the production of oxygen, nitrogen, liquefied natural gas, and olefins. As the most complicated and energy-intensive processes in CPI, ethylene plants normally use conventional vapor-compression cascade refrigeration system (CRS) for productions.

A CRS may include multiple refrigerants interexchanging heating/cooling loads among each other; meanwhile, each refrigerant has their own refrigeration cycles working at multiple temperature and pressure levels. Every subsystem/cycle contains a compression section, a condensing section, and several temperature levels with subcoolers (if exist), expansion valves, evaporators, and flash drums. Figure 1 illustrates two single-component cycles cascading to each other via a heat exchanger, which simultaneously acts as the evaporator of the higher-temperature cycle (the upper cycle, 5→6→7→8→5) and the condenser of the lower-temperature one (the lower cycle, 1→2→3→4→1). It should be noted that these two cycles may use the same refrigerant or different refrigerants operating at different pressures. In one cycle, the liquid refrigerant is first vaporized by isobaric heat absorption. Next, the vapor flows through an isentropic compressor to increase its pressure; then it is liquefied by isobaric cooling and isenthalpic expansion. This concept is normally represented by the *T–S* and *P–H* diagrams in literatures.[1]

Process synthesis and optimization of refrigeration systems have been studied in the last several decades. Barnés and King developed one of the earlier methods of identifying process configurations and selecting a refrigerant while minimizing costs using both heuristics and dynamic programming. They especially remarked how preliminary process analysis contributed in decreasing optimization complexity. [2] Later works in this field have also emphasized and elaborated this opinion. Following the case study in this article, Cheng and Mah[3] selected refrigerants based on a temperature range while using an interactive approach by linearization and ideal gas assumption for compressor energy balance. Another merit was their survey on a proposed extension to mixed refrigerant cycle. Meanwhile, a more theoretical method was introduced by Townsend and Linnhoff[4] using thermodynamic and heuristic principles to incorporate heat and power cogeneration by determining the placement of heat pumps and refrigeration systems to enhance thermal efficiency.

Mathematical programming-based refrigeration system synthesis was initially presented by Shelton and Grossman[5] as they introduced a simplified method of implementing saturated physical property into a mathematical model to avoid the usual complexity of the equation of state. They further developed a mixed-integer linear programming (MILP)

Correspondence concerning this article should be addressed to Q. Xu at Qiang.xu@lamar.edu.

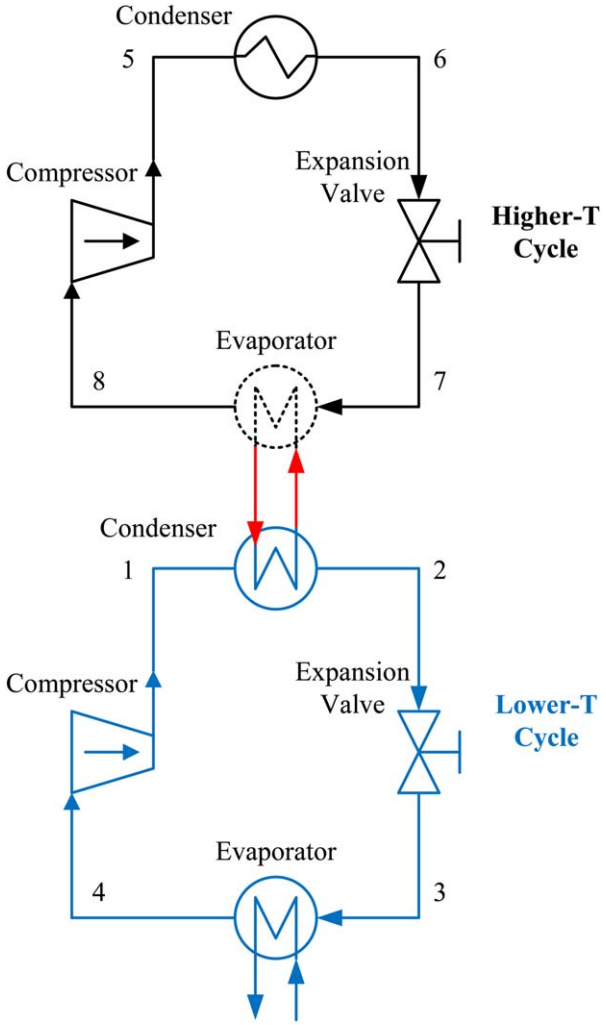

Figure 1. Sketch of two cascading single-component single-loop refrigeration cycles.

[Color figure can be viewed in the online issue, which is available at wileyonlinelibrary.com.]

model to optimize refrigeration cycle by optimizing a superstructure.[6] Colmenares and Seider[7] increased the scope of this work to a plantwide process synthesis that treated the whole plant as a large heat exchanger in a nonlinear programming approach instead. Another heuristics-based approach was from Raman and Grossman[8] as the process synthesis problem was solved as relaxed LPs instead of MILPs. The authors later implemented logic constraints and qualitative knowledge into the mixed integer non-linear programming (MINLP) model to further the search without violating global optimality in a quantitative framework with generic algorithms.[9] Vaidyaraman and Maranas[10] introduced a systematic methodology for multistage CRS synthesis and refrigerant selection as an MINLP problem with simplifications. Wu and Zhu[11] proposed the simultaneous process optimization and heat exchanger network (HEN) retrofit. Based on these approaches, Zhang et al.[12,13] developed global optimization synthesis models for refrigeration system with the existence of subcooler(s) and further addressed the chilling train operability in an ethylene plant.

Conversely, Wilson and Manousiouthakis[14] introduced the Infinite DimEnsionAl State-space (IDEAS) framework to the general process network synthesis problem, in which a globally optimal solution is achieved from an LP formulation. They then illustrated the applicability of the IDEAS framework to the solution of the minimum utility cost problem for multicomponent mass exchange networks. Pena-Lopez[15] demonstrated the applicability of the IDEAS approach to heat exchange network synthesis and refrigeration cycle synthesis. Mathematical programming-based process synthesis coupling with heat integration is always challenging tasks. Grossmann and coworkers presented a method to compensate these difficulties shown in the Duran and Grossmann work by handling both isothermal and nonisothermal streams.[16,17] Their approach used logic disjunctions and big-M constraints as proposing opportunity to reduce the MINLP model to an MILP model. In the last two decades, increasing efforts have been spent in developing algorithms to guarantee a global optimization search in such problem scale.[18–21] Besides, another mathematical approach by Holiastos and Manousiouthakis establishes, an optimal heat and power integration to minimize the overall utility cost without any prior commitment to a specific process design[22]; the resulting LP formulation was shown to identify that attaining the globally minimum utility cost may require that heat pumps not be placed across the pinch, as suggested by the Townsend and Linnhoff methodology.[4] Moreover, HEN design has also been refined by different methods, either integrating with the whole process,[23] or treating it as an independent problem.[24–28]

Exergy is defined as the maximum amount of useful energy from a process needed to bring a system to equilibrium with its surrounding environment. Exergy, denoted as B in this article, is quantitatively defined as the difference between enthalpy (H) and the product of entropy (S) and the ambient temperature T_a (Eq. 1). In other words, exergy is a property to evaluate the quality instead of the quantity of thermal duty in a system.

$$B = H - T_a S \tag{1}$$

In literature, exergy is separated into several categories, depending on either its causes or purposes. Cengel and Boles[29] categorized it as the amount of exergy transferred by work, heat or mass; while Aspelund et al.[30] classified exergy into components such as mechanic (potential and kinetic) and thermal (temperature-based, pressure-based, and chemical) exergy. In other words, exergy as a thermodynamic property can be supplied, transferred, or destroyed in different forms such as shaft work, kinetic energy, potential energy, internal energy, and enthalpy.[29] In a closed system, the lost/destroyed exergy and recovered/used exergy must add up to the total supplied exergy. Exergy losses, also known as irreversibility, happens to a heat engine as a result of an external physical impact (such as friction), composition changes (chemical reactions and mixing), heat transfer, or pressure-alternating equipments (compressor and expander). Exergy losses occur according to entropy generation and should always be positive. The thermodynamic analysis in this study pays more attentions in evaluating exergy changes due to temperature, pressure, and phase changes as well as mixing that usually happen in a CRS. To combine exergy analysis with mathematical modeling, Zhang and Xu[12] developed an exergy-embedded MINLP model for the optimal synthesis of a general CRS; they also used the exergy–temperature (B–T) chart to comprehensively analyze the thermodynamic nature of a refrigeration system. However, their

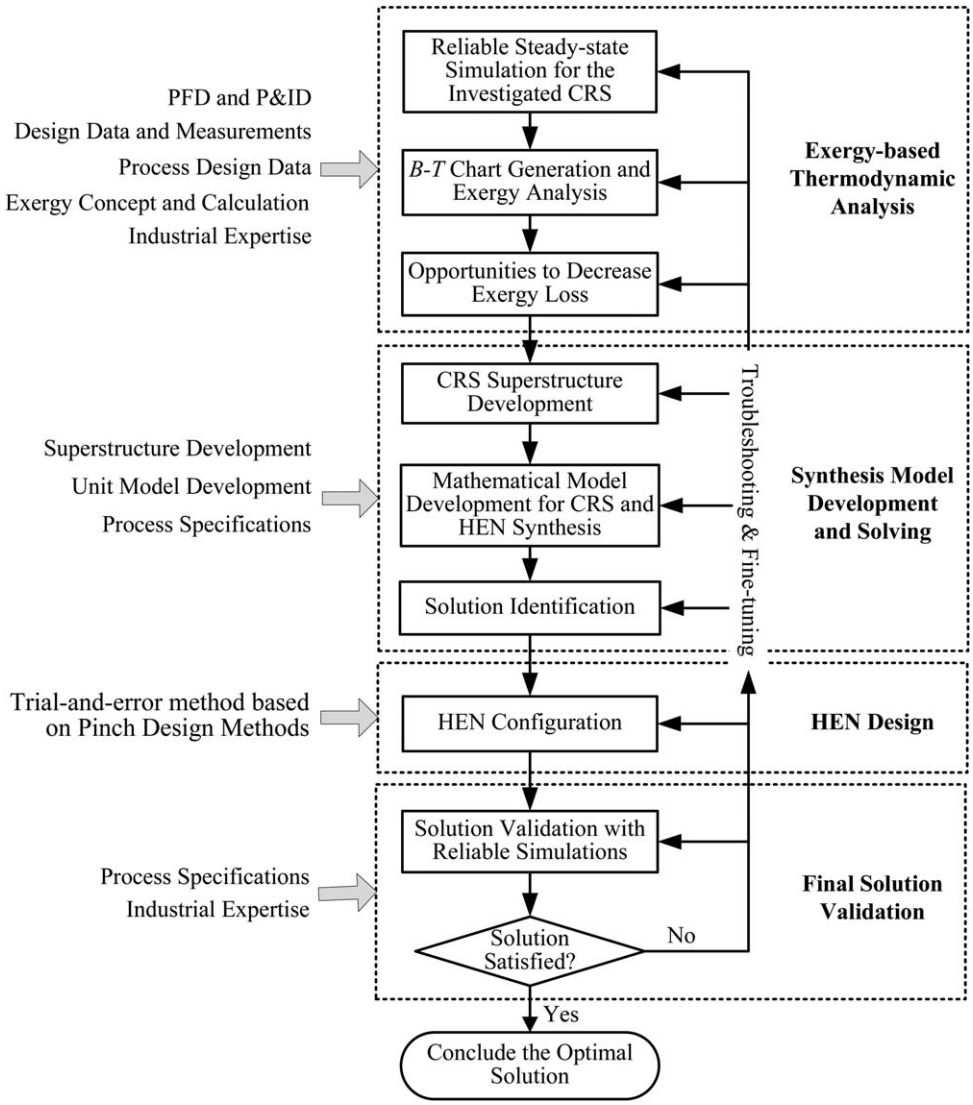

Figure 2. Methodology framework.

study did not cover the HEN design that is closely correlated to refrigeration system design and retrofit; meanwhile, their programming only considers stagewise subcooler options within each refrigeration recycles.

In this study, a general methodology is developed for the optimal synthesis of cascade vapor-compression refrigeration systems. The IDEAS approach can solve this problem[14]; however, another approach is introduced in this article to generate the optimization model according to the guidance of exergy analysis. The procedure of process synthesis involves four stages of work: (1) refrigeration system exergetic analysis, (2) optimization model development for simultaneous synthesis of refrigeration system and HEN; (3) HEN configuration identification; and (4) solution validation based on rigorous simulations. In the thermodynamic analysis, *B–T* chart from Zhang and Xu[12] is borrowed and extended to systematically analyze the CRS. An "IDEAS-based" MILP model is presented to minimize the total compressor shaft work of the HEN-considered refrigeration system, where multiple refrigerants with multiple recycling loops satisfying all of the process cooling demands are simultaneously addressed. Finally, the obtained optimal solution is examined by rigorous simulations to verify their feasibility and consistency.

Problem Statement

Given an appropriate refrigerant and a set of heating and cooling demands for several process streams coupling with their initial and targeted temperatures, the objective of this study is to obtain an optimal vapor-compression cascade refrigeration cycle together with an internal HEN configuration to minimize the total compressor work consumptions based on exergy analysis. This problem will be solved based on a process superstructure to determine the optimal pressure selection, the individual loop topology, the existence of interlevel subcoolers, as well as an embedded HEN configuration. The optimization problem is summarized as the following.

Assumptions

1. The refrigerant leaves condenser as saturated liquid and exits evaporators as saturated vapor; and

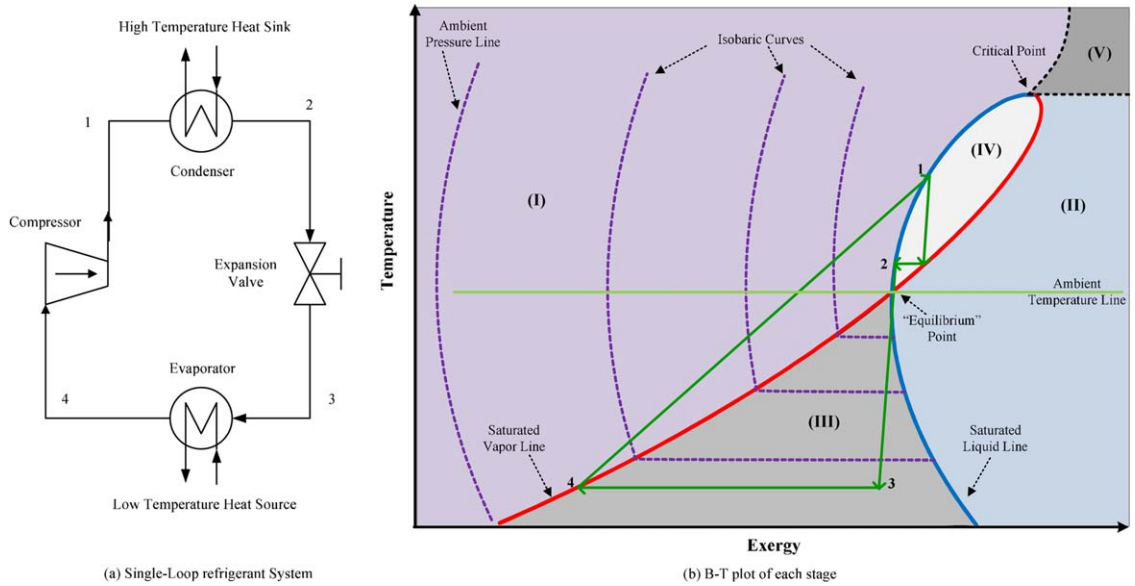

Figure 3. Sketch (a) and *B–T* chart (b) of a single-loop refrigeration system.

[Color figure can be viewed in the online issue, which is available at wileyonlinelibrary.com.]

2. Ideal gas behavior is assumed when necessary and an average heat capacity C_p is used to estimate the enthalpy changes within the temperature interval of a system.[29]

Given information

1. A set of process streams including their compositions, flow rates, and initial and targeted temperatures; and
2. A chosen refrigerant and its thermodynamic properties.

Information to be determined

1. A detailed structure of the entire refrigeration system including compressor and subcooler connections among levels;
2. Specific pressure levels used in the optimal refrigeration cycle;
3. The refrigerant flow rate at each unit;
4. Compressor shaft work; and
5. Heat loads in each subcoolers, condensers, and evaporators and their distribution within the HEN.

General Methodology Framework

The developed exergy-analysis-based optimization and process synthesis for a CRS involves four stages of work. Figure 2 presents their inclusive picture. First, a rigorous steady-state simulation model of the investigated refrigeration system is constructed based on the available process flow diagram, piping and instrumentation diagram (P&ID), and design data to carry out exergy-based thermodynamic analysis. Thermodynamic package and properties for the simulation should be appropriately selected at this stage. Since the scope of this methodology can be either as specific as within an ethylene plant (as in the case study if this article) or as extensive as any petrochemical process, the PR-BM (Peng-Robinson equation of state with alpha-function by Boston and Mathias[32]) property method is a favorable option. In the case study presented later, the widely accepted Peng-Robinson equation of state is used since separation on the lighter-hydrocarbon end is focused in ethylene plant simulation.[31] Moreover, the candidate levels of the operating pressure for a CRS are selected ranging from slightly above ambient to nearly critical conditions. Thus, BM alpha-function guarantees more precise calculation when the chosen level approaches the critical point.[32] System input information in this stage also includes both the refrigeration cycle itself and the heating/cooling demands covered by the studied plant CRS. Next, stream data will be extracted from the simulation model and exergy is calculated to generate a specific exergy path plotted in the *B–T* chart. This thermodynamic analysis helps to locate and evaluate exergy loss in the system; hence, opportunities to improve are expected to be explored and identified. During this stage, available inputs from industrial expertise/concerns are always encouraged, because the conclusive outcome serves as a backbone to generate a superstructure in the next stage.

In the second stage, a superstructure is developed from the conclusions drawn in the first stage. Based on material and energy balance of each unit and subsection in this superstructure, an MILP model coupling refrigeration system synthesis and associated HEN synthesis can be developed. The transshipment model for HEN synthesis is used.[33] It should be noted that the HEN synthesis involves the heating/cooling demands of process streams and some subcoolers/evaporators/condensers that are associated with structures and heat load distributions in the CRS. Thus, the refrigeration system and its associated HEN are better to be synthesized together for the sake of total energy savings. In the developed MILP model, the objective is to minimize the total shaft work consumptions; and equality and inequality constraints include mass and energy balances for each subrefrigeration system and various process specifications. The mathematical model is developed and solved in an optimization tool such as GAMS.[34] When the optimal solution has been identified, it suggests a set of chosen pressure levels for the studied CRS, their internal connections with subcooler(s) (if exists), refrigerant flow rates and operating temperatures at each unit, and the heat load distribution at each heat-exchanging allocation within the entire temperature range of HEN design. From this information, the number of hot and cold streams and their heat loads can be specified.

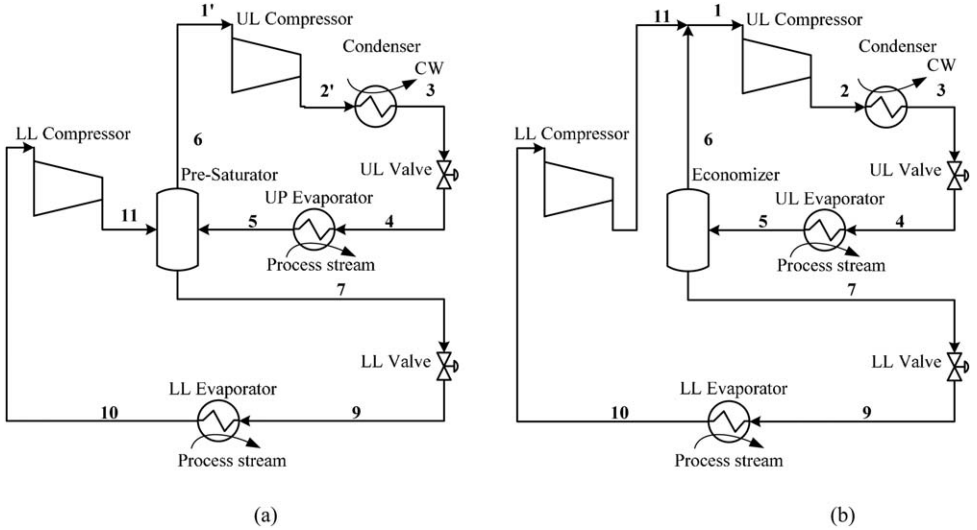

Figure 4. Sketch of a dual-loop refrigeration system with economizer (a) or presaturator (b).

A detailed HEN configuration will be identified in the third stage based on the obtained optimal solution. This HEN configuration is acquired through a manually trial-and-error technique according to the pinch design method originated by Linnhoff and Hindmarsh.[24] The optimization model also locates pinch point(s) in the networks, hence, dividing it into several subnetworks for a more convenient matching among hot and cold streams. Finally, in the fourth stage, the obtained final solution with detailed structure of the entire CRS and its associated HEN is examined by rigorous simulations to ensure its operational reliability. Possible troubleshooting may be performed in the prior stages of work, especially in the MILP model development and the HEN design stages, in case the validation results are not satisfied. The solution is considered creditable if it satisfies process requirements and answers to any industrial expertise knowledge if available. Iteratively, a final completed conceptual design/retrofit for the studied CRS and HEN system, including a detailed process configuration and operating information for every unit and stream, will be presented.

Exergy-Based Thermodynamic Analysis

B–T chart introduction based on a single-loop refrigeration system

The *B–T* chart has been proven as a valuable tool for thermodynamic analysis of refrigeration systems. Based on the example of Zhang and Xu,[12] Figure 3a shows the process sketch of a single-loop refrigeration system; while Figure 3b extends the thermodynamic representation for the pathway of specific exergetic flows within a single-loop refrigeration system. Similar to the conventional *P–T* or *H–T* charts, plotting the system exergetic pathway onto the *B–T* chart indicates both physical property and energy behavior of the system at every location.

In Figure 3b, the saturated vapor (plotted in red) and liquid (plotted in blue) lines of the refrigerant separate the *B–T* chart into five different regions. Region (I) on the left-hand side (LHS) of the vapor line indicates the superheated vapor phase. Any point in region (II) on the right-hand side (RHS) of the blue line is considered subcooled liquid. These two saturation lines intersect each other, creating two separating regions in between, the area underneath the intersection [Region (III)] and the one inside the loop [Region (IV)]. Region (III) is the only two-phase one in the chart; thus, any isobaric curve crossing it is a straight line indicating phase change by either evaporation or condensation, depending on the exergy flow direction.

Conversely, the refrigerant state in Region (IV) is identified according to the status of a specific point in the system. As seen in Figure 3a, Point 1 allocates compressor outlet, hence, implies superheated vapor at Region (IV) as the point lines on its relative isobaric curve. A point residing in Region (IV) indicates a current status of the fluid in a process depending on whether it belongs to an isobaric curve and its exact location referred to critical pressure line. Another significant feature in this chart is the intersection at the ambient temperature, where both states exist and the system neither releases nor accepts exergy when phase change occurs. Thus, this is considered an "equilibrium point" with respect to the ambience. Besides, the saturation lines are actually crossing only once at the ambient temperature, because their uppermost point is overlapped at the critical point, where saturated vapor and saturated liquid states are identical.[29] For other refrigerant such as ethylene when its "saturation peak" (critical point) is below the ambient temperature, the "equilibrium point" does not exist in its *B–T* chart. Region (V) indicates the supercritical phase, enclosed by isobaric and isothermal lines at the critical pressure and temperature. Liquid-phase exergy only varies to some extent with respect to pressure except the region around the critical point. Note that Figure 3b also provides highlighted features of the *B–T* chart with various isobaric curves.

Generally, the refrigerant dumps heat to a high-temperature heat sink (1→2) through a condenser, where the refrigerant drops its temperature and condensed to liquid. After it passes through the expansion valve, both pressure and temperature are significantly reduced (2→3). Next, the refrigerant goes through an evaporator to picks up heat and be vaporized at a low temperature (3→4). After that, the vapor refrigerant stream is compressed to the high level again by a compressor (4→1). Through such a closed-loop working procedure, heat is continuously transferred from the low-temperature source to the high-temperature sink at the

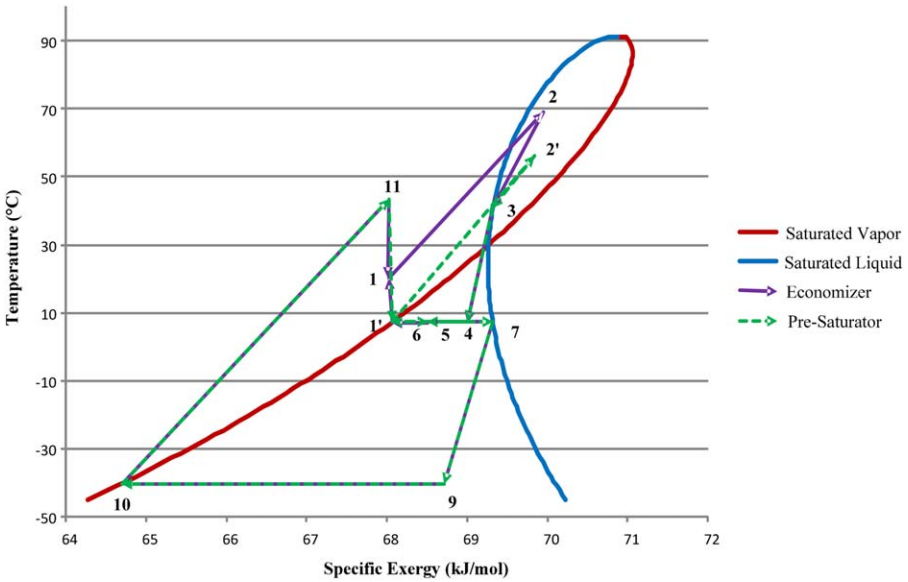

Figure 5. Specific exergy paths of the CRS represented in Figure 4.

[Color figure can be viewed in the online issue, which is available at wileyonlinelibrary.com.]

expense of the compression work, such that the heat source can be cooled down to a desired temperature. Obviously, 4→1 is the only step to increase the exergy of the refrigerant; while the other steps cause the exergy loss of the refrigerant.

Exergy distribution analysis and optimal opportunities for CRS

The main purpose of exergy-based thermodynamic analysis is to determine the exergy loss at each CRS operation step and consequently to identify opportunities for design and operational optimization. Figure 4 presents a simplified single-component dual-loop propylene refrigeration system to demonstrate the merits of exergy analysis. Figures 4a, b indicate two different processes at the intermediate pressure level connecting the upper-loop (UL) compressor and the lower-loop (LL) one. The LL has similar units (compressor, a condenser, an expansion valve) as the UL except the absence of a condenser. There are three pressure levels in this example, including the highest one at the UL condenser, the intermediate one at the flash drums (presaturator or economizer), and the lowest one at the LL evaporator. This arrangement represents the simplest structure of a multilevel refrigeration cycle.

Compression and condensation

In Figure 4, two most popular designs prior to the compressor inlet are the employment of either an economizer or a presaturator at intermediate levels, based on how the vapor flow is distributed in the system or whether saving compressor work is prioritized.[2,35] In both processes, the refrigerant after expansion and evaporation enters the flash drum (Stream 5) where isobaric phase separation takes place. The vapor stream from this unit (Stream 6) is fed to the UL compressor inlet while the liquid one (Stream 7) is directed to the LL expansion valve. The most significant structural difference between the two designs is the destination of the interlevel compressor outlet (Stream 11). In the CRS with the economizer design (Figure 4b), the superheated vapor Stream 11 is mixed with the drum outlet (Stream 6) before entering the UL compressor as Stream 1. However, in the other CRS (Figure 4a), the presaturator receives Stream 11 before flashing; hence, Streams 6 and 1 are identical. Both design configurations imply intermediate pressure levels, which is also the basis of defining a superstructure. The economizer provides higher temperature at UL compressor inlet, which is insignificant from the viewpoint of refrigeration efficiency. As stated by Barnes and King,[2] the mixing of vapor streams at different temperatures increases the system entropy and decreases its thermodynamic efficiency. Hence, when this phenomenon occurs inside a flash drum, more vapor is produced to feed to UL compressor. As a result of this, presaturator has less liquid refrigerant directed to the lower-pressure (colder) level, which is not in favor for this loop to fulfill its cooling demands.

It should be noted that since the highest pressure level in the refrigeration cycle is set at the condenser, where superheated vapor from compressor is completely liquefied. Exergy loss across this point (2 (or 2′)→3) is demonstrated in two types: temperature drop and phase change. This is inevitable and cooling water is considered an external utility, as most refrigerants in an ethylene plant have dew points far below ambient conditions. Besides, a CRS with multiple compression levels also have more application flexibility compared with a single-stage system. Although one large compressor is more economic than having several compressors in terms of requiring smaller total shaft work, it is a user-determined tradeoff in this synthesis concept. Note that the amount of supplied exergy to a CRS due to compressions is equal to the summation of exergy destroyed/lost through

Table 1. Comparison of Two CRS Designs Based on the Same UL $COP_{heating}$

Comparison	Economizer	Presaturator
Outlet flows of flash drum to adjacent stages	More liquid	More vapor
Upper-loop compressor outlet temperature	Higher	Lower
Lower-loop $COP_{cooling}$	Higher	Lower

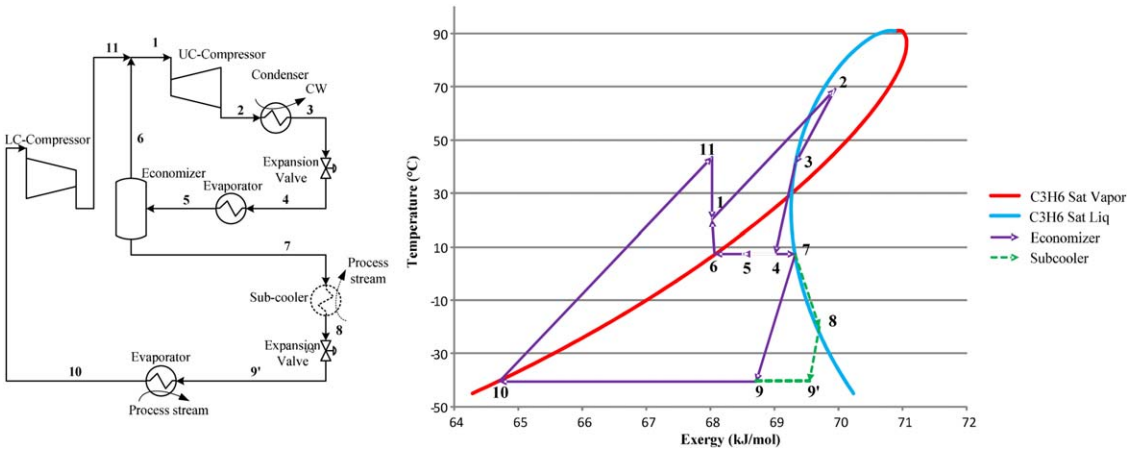

Figure 6. Sketch (a) and specific exergy paths (b) of a dual-loop refrigeration cycle with and without a subcooler in the LL.

[Color figure can be viewed in the online issue, which is available at wileyonlinelibrary.com.]

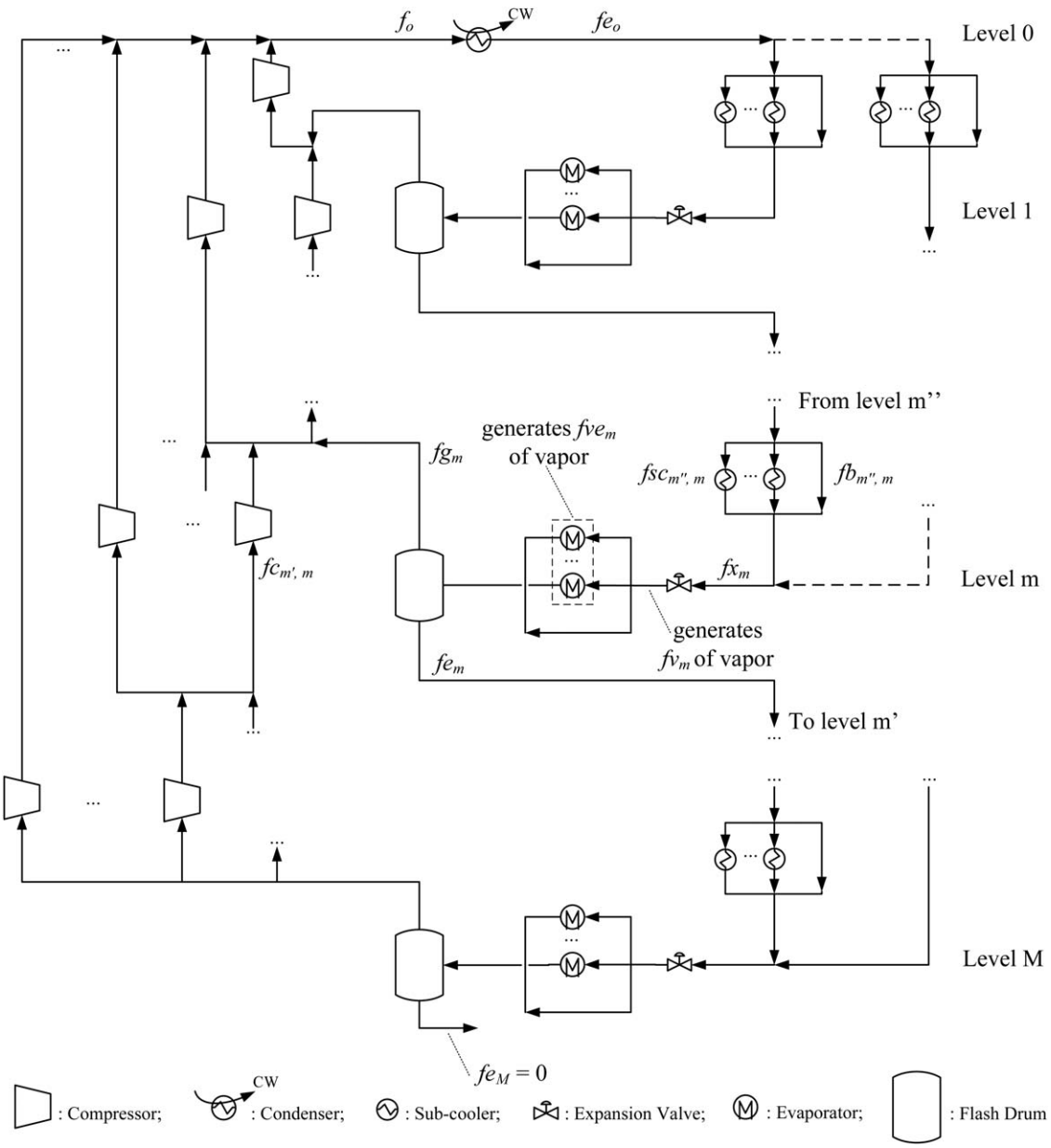

Figure 7. The superstructure of a single-component multilevel CRS.

operation and exergy transferred by heat exchangers (subcoolers, evaporators, and condensers). Hence, considering a CRS as a whole, either shaft or electrical work is equivalent to the supplied exergy; meanwhile the transferred exergy is a constant, which is equivalent to the customized process energetic demands. Therefore, it can be inferred that minimizing compressor work is equivalent to minimizing exergy loss in a CRS.

Figure 5 shows a *B–T* chart of the CRSs represented in Figure 4. The plot suggests the same supplied exergy for both designs in Figure 4, which takes place during compression actions (10→11 and 1(1′)→2(2′)). The outlet temperature of the UL compressor in the economizer design (Figure 4a) is approximately 10°C higher than the same stream property (see 2 vs. 2′ in Figure 5) in the presaturator design (Figure 4b). However, because cooling water in the condenser immediately liquefies this stream, this temperature increment does not affect the overall CRS efficiency. It should be pointed out that the horizontal axis of Figure 5 is defined by molar specific exergy (kJ/mole). Thus, although both designs in Figure 5 have identical specific exergy pathways in some operation sections, their exergy loads are different due to different refrigerant flow rates in each loop. Significant features are compared between two designs in Table 1, where the comparison is based on both designs having the same coefficient of performance ($COP_{heating}$) in their UL. Here, $COP_{heating}$ and $COP_{cooling}$ are defined below

$$\text{Refrigerator } COP_{cooling} = \frac{\text{Received Heat}}{\text{Added Work}} = \frac{Q_C}{W} \quad (2)$$

$$\text{Heat pump } COP_{heating} = \frac{\text{Released Heat}}{\text{Added Work}} = \frac{Q_H}{W} \quad (3)$$

From Table 1, the merit of using the economizer design lays in its ability to deliver more liquid refrigerant to the lower-pressure level, thus resulting in larger Q_C and higher $COP_{cooling}$ in the LL and satisfying refrigeration cooling demands in a low-temperature range. In Figure 5, the economizer results in higher outlet temperature of the higher-pressure level compressor (at point 2 comparing to 2′). However, the projected distance on the specific exergy axis does not vary between these two designs; hence, presaturator delivers a higher flow rate to the UL compressor, implying larger shaft work required. In summary, the CRS with economizer design is more preferred in the CRS superstructure development.

Expansion and subcooling

Expansion through Joules–Thompson valve causes pressure drop. It also induces a large amount of exergy loss in a refrigeration cycle. This step occurs at a constant enthalpy since there is neither heat nor work delivered to the refrigerant. Pressure drop causes temperature decrease and partial vaporization to the refrigerant at the saturated liquid status. When the refrigerant stream passes through an expansion valve, its temperature can drop far below the ambient temperature associated with its pressure drop; hence, this stream has increased the potential cooling capacity. In other words, some quantity of pressure exergy is converted to temperature exergy.[30] Conversely, based on the *B–T* analysis from Zhang and Xu,[12] an addition of a subcooling action is to minimize this exergy loss. As previously demonstrated, an economizer is better to be adopted in the dual-loop cycle and a subcooler is located prior to the LL expansion valve (Figure 6a). Its relative exergetic pathway in Figure 6b indicates that the employment of a subcooler can partially recover the exergy loss (7→9); and in the meantime, it can increase the cooling capacity at the LL evaporator (9→9′). Note that the subcooler placement has been elaborated in details within mathematical modeling in the later context because it is directly related to each level's existence.

Evaporation and the HEN

A refrigeration system serves the purpose of delivering excess heat from one source in a process to another sink to satisfy both heating and cooling demands. Thus, the evaporators are considered to be where a CRS reflects its cooling potential fully. Refrigerant enters the evaporators of a pressure level at its saturated temperature and is vaporized by heat transferred from the process side. Within each unit, the refrigerant acts as the cold stream while a process stream acts as the hot stream; hence, a CRS should be able to provide a quantity exceeding or at least equal to the process' cooling demands. A CRS and its relatively served process streams can be considered as an HEN in general, whose inputs include process heating and cooling demands and the available refrigerant streams flowing through both subcoolers, evaporators, and condensers. Regarding the HEN synthesis, the transshipment model introduced by Papoulias and Grossman gives the energy balance at the *j*th temperature interval (Figure 7) as[33]

$$R_j - R_{j-1} + U_{Hj} - U_{Cj} = Q_{Hj} - Q_{Cj} \quad (4)$$

where R_{j-1} is the residue heat passing from the higher-temperature interval; and R_j is the unused amount cascading down to its following; U_H and U_C are duties supplied from hot and cold utilities, while Q_H and Q_C are the heat exchanged by process hot and cold streams, respectively.

MILP Model Development

Process superstructure development

The superstructure representation in Figure 9 shows all possible connections among higher- and lower-pressure levels. It considers three general scenarios on how saturated refrigerant liquid from a condenser or an economizer leaving from a chosen level can be directed to the next level(s):

1. flows to the next evaporation section by passing a subcooling section (named as interlevel subcooler). Note that subscenarios with or without subcoolers are both considered.
2. bypass the next evaporation section(s) through a so called cross-level subcooling section and directly flows to evaporation section(s) of even lower-pressure levels.
3. simultaneously considering (1) and (2) by splitting the refrigerant liquid from the condenser or an economizer.

For the compression section, it also contains all possible design scenarios. Vapor streams from an economizer can be compressed to either one or multiple higher-pressure levels. A refrigerant is selected so that its temperature window from the ambient to the critical pressure can cover the initial and targeted temperatures of the given process streams. A combination of all possible pressure levels $SM = \{m|0, ., M\}$ are assumed as the candidates for optimizing the superstructure. Based on the superstructure shown in Figure 7, an MILP model including material and energy balance of each unit operation per loop with equality and inequality constraints

by considering all the design possibilities will be developed and solved. Note that in addition to process demands, rigorous steady-state simulations should be used to provide thermodynamic data and parameters as inputs to the mathematical model.

Mass balance equations and constraints

Compression is modeled according to the conclusion in the above exergy-based thermodynamic analysis, where mass balance around each compressor is determined based on the economizer design. Equation 5 characterizes this relation.

$$fg_{m-1}+\sum_{m'=m+1}^{M} fc_{m',m}=\sum_{m''=0}^{m-1} fc_{m,m''}\ ,\forall\ m\in SM \quad (5)$$

where $fc_{m',m}$ is the mass flow rate through the compressor from the lower-pressure level m' to the current one m; $fc_{m,m''}$ is the mass flow rate leaving the compressor from the pressure level m to the upper one m''. In Eq. 5, the LHS represents the inlet flow rate of a compressor at the pressure level m, which is the summation of the saturated vapor from the $(m-1)$th pressure level flash drum (fg_{m-1}) and the total superheated vapor from the lower-pressure level compressors ($fc_{m',m}$). The RHS of Eq. 5 represents a summation of the feed rates of compressor outflows, which may be directed to higher-pressure level compressors.

Equations 6 through 9 introduce a binary variable y_m to present whether the mth pressure level exists. y_m equals to 1 when the mth pressure level exists; otherwise, it is 0. Z is a sufficiently large scalar. Equation 8 guarantees that there is no reverse flow through a compressor from a higher-pressure level to a lower one. Equation 9 limits the maximum number of existing pressure levels. Note that the condenser is assigned as the zeroth level, considerably the highest pressure within the whole cycle. Since the condenser always exists, Eq. 10 always holds true. Equation 11 indicates that f_0 is the largest flow rate variable in the cycle and is essentially defined as the total refrigerant amount circulating in the studied cycle.

$$fc_{m',m}\le y_m\ Z,\quad \forall m\in \mathrm{SM},\quad \forall m'\in \mathrm{SM},\ m'>m \quad (6)$$

$$fc_{m,m''}\le y_m\ Z,\qquad \forall m\in \mathrm{SM},\ \forall\ m''\in \mathrm{SM}, m''<m \quad (7)$$

$$fc_{m',m}=0,\forall\ m'<m \quad (8)$$

$$\sum_{m=1}^{M} y_m\le M \quad (9)$$

$$y_0=1 \quad (10)$$

$$\sum_{m=1}^{M} fc_{m,0}=f_0 \quad (11)$$

While a compressor links the working fluid traveling from a lower-pressure level to a higher-pressure one, the saturated liquid leaving a higher-pressure level reaches the lower one(s) by passing through either subcooling section(s) (if exists) or only an expansion valve. Mass balance are carried out for all of those possible scenarios whether or not a subcooling section exists between any two levels in the following equations

$$fe_m=\sum_{m'=m+1}^{M}\left(f\mathrm{sc}_{m,m'}+fb_{m,m'}\right),\quad \forall\ m\in \mathrm{SM},\ m<M \quad (12)$$

$$fx_m=\sum_{m''=0}^{m-1}\left(f\mathrm{sc}_{m'',m}+fb_{m'',\ m}\right),\quad \forall m\in \mathrm{SM},\ m<M \quad (13)$$

where fe_m is the flow rate of the saturated liquid stream from a flash drum at the m-th pressure level; fx_m is the total flow rate passing through the evaporation section to enter this flash drum; $f\mathrm{sc}_{m'',m}$ and $f\mathrm{sc}_{m,m'}$ represent flow rates through subcooling sections entering and leaving the mth pressure level; and $fb_{m'',\ m}$ and $fb_{m,m'}$ represent flow rates through bypass line entering and leaving the mth pressure level. The LHS of both Eqs. 12 and 13 refer to the total inlet flow and the liquid outlet flow of the flash drum, respectively.

It should be noted that only one variable between each pair of $f\mathrm{sc}_{m,m'}$ and $fb_{m,m'}$ can be active: that is, if one exists, the other must be zero. Similarly, only one variable of each pair of $f\mathrm{sc}_{m'',m}$ and $fb_{m'',\ m}$ can be active. Such existence constraints are implemented in Eqs. 14 through 17.

$$f\mathrm{sc}_{m,m'}\le y_m\ Z,\qquad \forall\ m,\ m'\in \mathrm{SM},\ m<m' \quad (14)$$

$$fb_{m,m'}\le y_m\ Z,\quad \forall\ m,\ m'\in \mathrm{SM},\ m<m' \quad (15)$$

$$f\mathrm{sc}_{m,m'}=0,\quad \forall\ m,\ m'\in \mathrm{SM},\ m>m' \quad (16)$$

$$fb_{m,m'}=0,\quad \forall\ m,\ m'\in \mathrm{SM},\ m>m' \quad (17)$$

In particular, $f\mathrm{sc}_{m,m'}$ is the necessary amount of refrigerant to provide heating duty to a certain process demand(s); thus, a subcooling section can contain one or several heat exchangers arranged in parallel or in series. The detailed orientation depends on the result from the HEN configuration synthesis. In addition, fv_m, the amount of vapor generated by an expansion valve at the mth pressure level, is calculated as a product of the valve inlet flow rate $fb_{m'',m}$ from the higher-pressure level(s) and the vapor fraction $\mathrm{vf}_{m'',m}$ when a pressure drop from the m''th pressure level to the mth one is taken into account, as shown in Eq. 18.

$$fv_m=\sum_{m''=0}^{m-1} fb_{m'',m}\ \mathrm{vf}_{m'',m},\qquad \forall\ m\in \mathrm{SM} \quad (18)$$

Hence, the refrigerant continues passing through the mth pressure level evaporation section as a vapor-liquid mixture and goes through phase separation in the adiabatic flash drum. Equations 19 and 20 define the outlet streams of the mth pressure level economizer, in which a flash separation takes place.

$$fg_m=f\mathrm{ve}_m+fv_m,\quad \forall\ m\in \mathrm{SM},\ m>0 \quad (19)$$

$$fe_m=fx_m-fg_m,\quad \forall\ m\in \mathrm{SM},\ m>0 \quad (20)$$

where $f\mathrm{ve}_m$ is a dependent variable indicating the total flow rate of saturated vapor produced by evaporation at the mth pressure level. If the process cooling demand is less than the available supply by the refrigerant amount passing through the evaporation section at this level, a bypass line is included for the excess refrigerant stream. Similar to the subcooling section, the exact placement of the heat exchangers acting as evaporators at each pressure level is finalized during the HEN configuration synthesis. Besides, the equality constraints of Eqs. 21 and 22 specify that the refrigerant flows within a closed-loop CRS system.

$$fe_0=f_0 \quad (21)$$

$$fe_M=0 \quad (22)$$

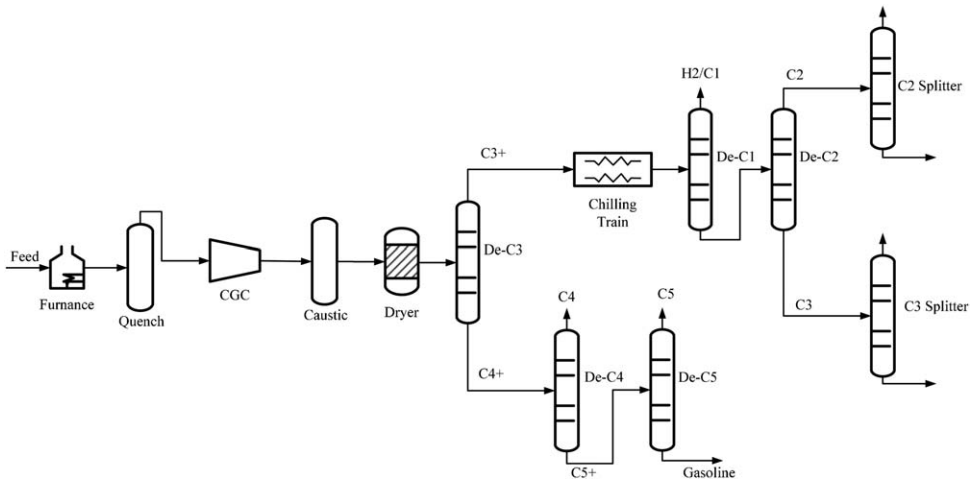

Figure 8. Sketch of the studied front-end depropanizer ethylene plant.

Energy balance of the embedded HEN and the compression section

The major heat integration opportunities in a CRS are to satisfy the heating demands of process streams by implementing subcoolers and the cooling demands using refrigerant evaporators. The condenser energy performance is not included in modeling the energetic targets of the embedded HEN, because it dumps heat to either utility streams such as cooling water or another refrigerant cycle and consequently has no contribution in fulfilling the refrigeration demands of the process streams with respect to the considered CRS cycle. All of subcoolers and evaporators in the superstructure-based synthesis model are considered as parts of the embedded HEN associated with the studied refrigeration cycle. As the previously stated, the given hot-process streams and refrigerant streams passing through a subcooling section (if available) define the HEN hot-side streams; while the given cold-process streams and the refrigerant streams passing through evaporators are assigned as the HEN cold-side streams. A collection of the inlet and outlet temperatures of both hot-side and cold-side streams divides the temperature range of the whole CRS into a series of continuous temperature intervals, which is indexed as $\mathrm{SJ} = \{j|0,\ldots,J\}$. A minimum temperature difference in each exchanger should be given to avoid temperature cross-over between hot-side and cold side streams. Besides, although an evaporation section is assumed to be isothermal, a small temperature increment (0.2°C) is introduced in each evaporation section in this study to ensure a temperature interval is relative to an evaporator section.

The total heat duty Qx_m of all evaporators in the mth level is calculated by their vapor flow rate multiplied by the specific heat of vaporization $\Delta\mathrm{hr}_m$ at that particular pressure, as shown in Eq. 23. Ideal gas behavior is assumed for the vapor refrigerant in evaporation section, thus, the enthalpy change $\Delta\mathrm{hr}_m$ is considered a function of temperature. Equation 24 is a constraint to assign this heat duty as zero if its relative level is not selected.

$$Q\mathrm{x}_m = f\mathrm{ve}_m\ \Delta\mathrm{hr}_m, \quad \forall\ m \in \mathrm{SM},\ m > 0 \tag{23}$$

$$Qx_m \leq y_m\ Z,\ \forall\ m \in \mathrm{SM},\ m > 0 \tag{24}$$

To ensure the refrigeration cycle works properly, the total amount of Qx_m needs to be larger than or at least equal to the cooling demands of process streams. This HEN synthesis transshipment model and energy balance in Eq. 25 at the jth interval are in a similar manner as demonstrated in Eq. 4.

$$R_j - R_{j-1} + \sum_{m''=0}^{m-1}\sum_{m=1}^{M} Q\mathrm{sc}_{j,m'',m} f\mathrm{sc}_{m'',m} \mathrm{Cp}(T_m - T_{m''}) - \sum_{m=1}^{M}\left(Qx_m xi_{j,m}\right) = \sum_{n=1}^{N} Qh_{j,n} - \sum_{l=1}^{L} Qc_{j,l}\ ,\ \forall\ j \in \mathrm{SJ} \tag{25}$$

where $R_j - R_{j-1}$ is the used heat residue in the jth temperature interval the HEN. The third item of LHS indicates the heating duty provided by the refrigerant from all subcooling sections for the jth temperature interval; and the last item of the LHS indicates the net cooling duty supplied by the refrigerant from all evaporation sections that exist for the temperature interval. These two items can be considered as the heat supplies of the hot and cold utilities as shown in Eq. 4. Here, $Q\mathrm{sc}_{j,m'',m}$ is a dimensionless heat fraction indicating a ratio of heating duty provided by the refrigerant in a subcooler from level m'' to level m and contributed to the process side within this jth temperature interval. Note that the third item of the LHS is determined under the Assumptions (1) and (2) using the average heat capacity C_{P}, which can be attained from a thermal property database.[36] Since the refrigerant is completely liquefied and assumed to leave the condenser as saturated liquid, a constant heat capacity can be used to calculate the amount of heat transferred from the liquid refrigerant to the process side across a subcooling section. In the fourth item of the LHS, $xi_{j,m}$ is an binary index vector indicating whether the saturated temperature of the mth level crosses this temperature interval. On the RHS of Eq. 25, the heat inputs $Qh_{j,n}$ and $Qc_{j,l}$, defined in the same manner as Q_{Hj} and Q_{Cj} in Eq. 4, are summations of heating demands from cold process stream l and cooling demands from hot process streams n in temperature interval j, respectively. It should also be noted that the set of hot process streams $\mathrm{PH} = \{n|1,\ldots,N\}$ and the set of cold process streams $\mathrm{PC} = \{l|1,\ldots,L\}$ are initially given information.

Table 2. Given Information of Process Streams Served by the Propylene Refrigeration System

Stream ID	Related Unit ID	Related Unit Type	Inlet T (°C)	Outlet T (°C)	Q (GJ/h)	Related Unit Descriptions
1	CO-1	Cooler	−36.0	−35.8	0.03	Evaporator of liquid ethylene from storage
2	CO-2	Cooler	−6.1	−5.9	7.01	De-methanizer (De-C1) reboiler
3	CO-3	Cooler	16.0	16.2	1.92	De-methanizer stripper reboiler
4	CO-4	Cooler	−29.3	31.8	2.20	Cold box #1
5	CO-5	Cooler	−26.9	30.0	1.10	Ethane product from C_2 splitter heater
6	E-1	Evaporator	−35.8	−36.0	18.54	De-ethanizer (De-C2) condenser
7	E-2	Evaporator	−9.8	−33.5	15.18	High-pressure de-propanizer reflux chiller #5
8	E-3	Evaporator	−24.5	−34.4	12.94	Ethylene condenser
9	E-4	Evaporator	10.0	−11.0	2.15	Ethylene desuperheater #2
10	E-5	Evaporator	16.0	−8.3	11.70	High-pressure de-propanizer (HP De-C3) feed chiller
11	E-6	Evaporator	1.4	−9.8	8.34	High-pressure de-propanizer reflux chiller #3
12	E-7	Evaporator	12.1	11.0	0.04	Low-pressure de-propanizer (LP De-C3) condenser
13	E-8	Evaporator	33.4	10.0	2.40	Ethylene desuperheater #1
14	E-9	Evaporator	33.0	12.8	11.72	Dryer feed chiller No. 2
15	E-10	Evaporator	37.4	27.0	1.92	High-pressure de-propanizer reflux chiller #1
16	E-11	Evaporator	43.3	33.0	3.81	Dryer feed chiller #1
17	E-12	Evaporator	67.8	28.0	0.36	Methanator effluent subcooler #2

Additionally, the logical constraints as shown in Eqs. 26 through 28 are necessary to guarantee that the HEN can supply to the energy requirements of the studied process system. According to the second law of thermodynamics, the exiting residue heat is defined as positive across every interval except the first and the last ones, since the problem is defined as no utility used and the refrigerant is treated as either hot or cold streams in the HEN configuration.

$$R_j \geq 0, \quad \forall j \in J \tag{26}$$

$$R_0 = 0 \tag{27}$$

$$R_J = 0 \tag{28}$$

The total compressor work consumption is determined collectively from a summation of all individual compression between two intermediate stages. Such variable $W_{m',\ m}$ is the

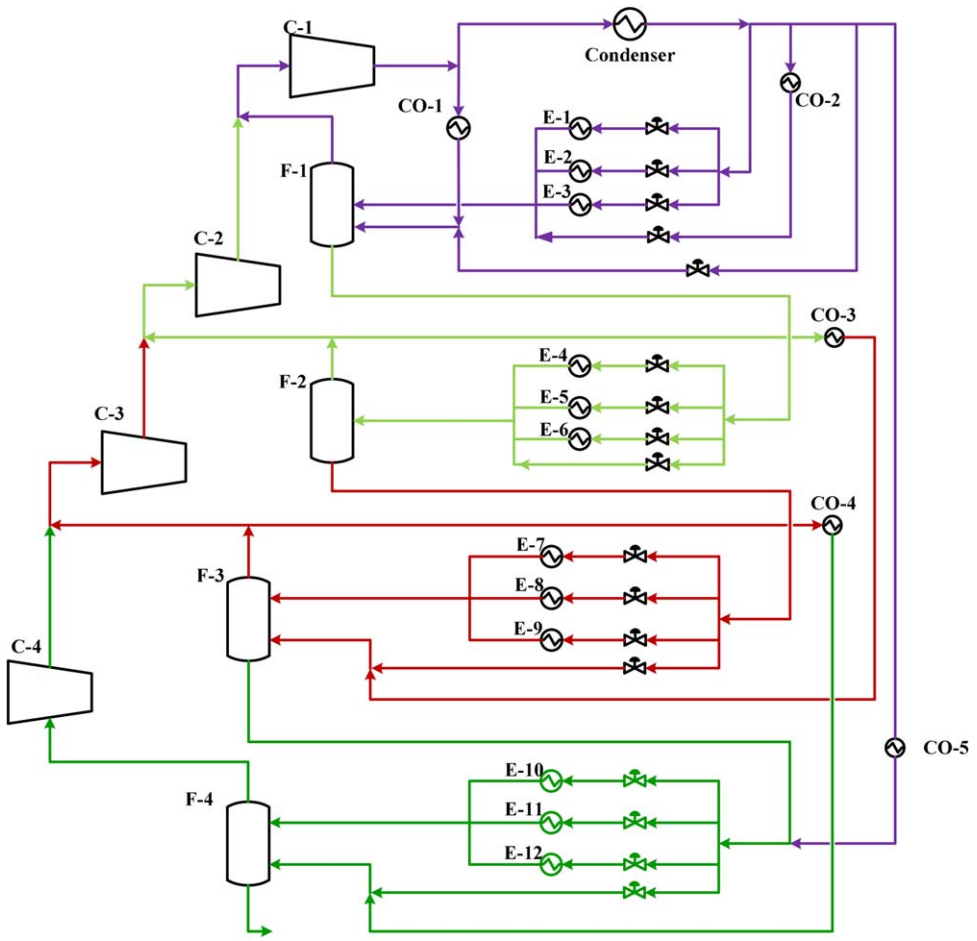

Figure 9. Base case design of the propylene refrigeration cycle in the studied ethylene plant.

[Color figure can be viewed in the online issue, which is available at wileyonlinelibrary.com.]

resulted work spent on the compressor connecting the pressure level m' to the pressure level m

$$W_{m',m} = fc_{m',m}\ \mathrm{wf}_{m',m}, \quad \forall\ m, m' \in \mathrm{SM};\ m < m' \qquad (29)$$

where $wf_{m',m}$ is a parameter representing the specific compressor work from pressure levels m' to m. This value is achieved by rigorous simulation with an assumption of 72% of compressor efficiency and $W_{m',\ m}$ is assigned as a positive variable to avoid the second law violations. The total compressor work consumption (TotW) in the whole CRS is calculated as the sum of all possible connections from the lower levels to their higher ones, including both interlevel and cross-level compressor stages,

$$\mathrm{TotW} = \sum_{m'=m+1}^{M} \sum_{m=0}^{M} W_{m',m} \quad \forall\ m, m' \in \mathrm{SM};\ m < m' \qquad (30)$$

The summary of the MILP model

The objective function of this problem is to minimize the total compressor work consumption (TotW) in the whole CRS, which is defined by Eq. 30.

$$\begin{aligned}
&min\ (30)\\
&s.t.\ (5, 12, 13, 18-20) && \text{Mass balance of each unit operation}\\
&\quad (25) && \text{Energy balance the HEN}\\
&\quad (8, 10-11, 16-17, 21-23, 27-30) && \text{Equality constraints}\\
&\quad (6-7, 9, 14-15, 24, 26) && \text{Inequality constraints}
\end{aligned} \qquad (31)$$

In this mathematical model, the variables, which include stream flow rates, exchanged heat in the HEN and the calculated compressor work, are defined by mass and energy balance around each unit operation. The minimizing target of the optimization problem, the compressor work utilization, is directly proportional to the flow rate across each unit, according to Eqs. 29 and 30. The mass balance around each unit operation is formulated in linear relationship among the flow rate variables within the working fluid distribution throughout the CRS model. The energy balance presented by the transshipment model in Eq. 25 also indicated that the variable Qx_m is also directly related to the flow rate $fsc_{m'',m}$ when the other terms are problem inputs extracted from the steady-state simulation model at the first stage of this methodology. The inequality constraints guarantee the variable existence and logic while the equality constraints present bounds at the structure extreme locations. Hence, an MILP model is achieved and solved for an optimal design of a CRS with an embedded HEN from the determined superstructure in Figure 7.

Case Study: Retrofitting a Propylene CRS in an Ethylene Plant

Base case and the MILP model inputs

The proposed methodology and MILP model is demonstrated by a case study of retrofitting the propylene refrigeration cycle (named as C3 CRS in this study) in an existing ethylene plant. This studied plant is a front-end de-propanizer ethylene plant with an adequate productivity of propylene. Figure 8 shows a simplified flow diagram of this process. Its recovery section starts with a de-propanizer (De-C3) column to separate the C_3's and lighter components to the light-end and the C_4's and heavier ones to the heavy-end. Detailed process stream data such as locations, temperatures, and their respective required heat duties, are listed in

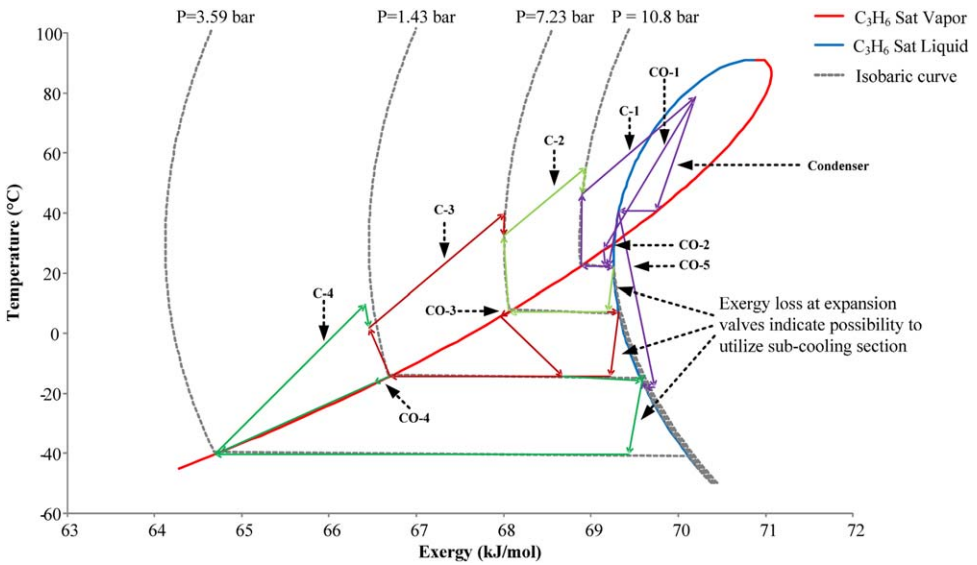

Figure 10. *B–T* plot of the base case design of current C3 CRS.

[Color figure can be viewed in the online issue, which is available at wileyonlinelibrary.com.]

Table 3. Candidate Pressure Levels Used in the Optimization Model

m	0	1	2	3	4	5	6	7	8
P_m (bar)	16.93	13.87	10.81	9.04	7.27	5.50	3.73	2.58	1.43
T_m (°C)	40.90	32.28	22.14	15.26	7.30	−2.26	−14.50	−25.11	−40.30

Table 2, including five hot streams and 12 cold streams (accordingly, $N = 5$ and $L = 12$). Because of the availability of high propylene flow rate in the C3 Splitter product stream, this C3 CRS contributes a great part in supplying duties to several condensers and reboilers of the distillation columns in the recovery section as well as satisfying the cooling demand of the chilling train to achieve cryogenic separation between hydrogen and ethylene. In this study, the base case is the plant existing C3 CRS design. Its energy demands and process stream data are fixed as inputs to the optimization synthesis model.

As seen in Figure 9, the base case of the investigated propylene refrigeration cycle contains a four-stage compressor system working at four pressure levels, a condenser at the highest pressure, and a combination of heat exchangers acting as coolers and evaporators. The highest pressure of propylene stream across the condenser is 16.93 bar, which is also assigned as the zeroth pressure level. This condenser uses cooling water as utility. The original C3 CRS contains 17 heat exchangers (Table 2), five of which are coolers and 12 are heaters with respect to the propylene refrigerant. It should be noted that the base case also adopt the economizer design at the flash drum allocations.

Based on available historian data, a rigorous steady-state simulation for the C3 CRS cycle of the base case generates the *B–T* plot shown in Figure 10, where specific exergy pathways of the refrigerant flows are plotted in similar colors corresponding to the process diagram in Figure 9. It can be seen that the expansion lines of valves have significant horizontal projectiles in the negative direction of exergy change, indicating quantities of exergy loss. Thus, the C3 CRS cycle may provide some extra heating duties to process streams through introducing a subcooling operation before those pressure expansion valves. Meanwhile, the allocation of some coolers in the base case also suggests some certain chances of exergy loss. The "CO-1" cooler simultaneously functions as a partial condenser and a subcooler for the propylene refrigerant. However, the amount of exergy loss by the condensation action exceeds the exergy gained from the subcooling and mixing action after this heat exchanger. Besides, the cooling action by the "CO-4" unit causes quite an exergy loss at the mixing point prior to the "C-4" compressor inlet. The *B–T* plot also implies some opportunities to improve the refrigeration system performance such as: (1) an addition of a subcooling section can use the aforementioned heating duty and increase the C3 CRS efficiency; (2) the existing setting of pressure levels may not be the best choice to achieve best COP in the CRS; and (3) an adjustment in flow rate distribution may contribute in saving the compressor shaft work consumption. Hence, these observations motivate the CRS optimization based on the proposed methodology.

In Table 3, four additional candidate pressure levels ($m = 1, 3, 5, 7$) are added into the base case design by averaging values of two consecutives among the existing pressure levels (the zeroth, second, fourth, sixth, and eighth levels) to obtain an optimal structure, thus, $SM = \{0, 1, ., 8\}$. Saturated temperatures at each level are also known, which is defined by the bubble point at its relative pressure level. Consequently, temperature levels determine candidate evaporators' temperature on the refrigerant side. Ambient temperature is still assigned as 30°C. The minimum temperature approach in the HEN is 2°C. An increment of 0.2°C is assumed for refrigerant vapor exiting an evaporator. Based on the developed MILP model, the model has 697 equations, 435 variables, and eight binary variables and is formulated in GAMS and optimized by the commercial solver of BARON.[34,37] The solution is obtained in a 64-bit Intel Dual-Core 3.40 GHz Dell computer in 0.03 s.

Optimal Retrofit Solution. The results of the optimal case are summarized in Tables 4 through 6. The optimization model chooses the intermediate levels (levels 4, 6, and 7) at lower pressures comparing to the existing levels in the base case, saving 17% in total shaft work consumption. Beside, in the optimal case, more than 50% of the total compressor work is consumed at the second highest level ($m = 4$), where

Table 4. Design Solution Comparison Between the Base and Optimal Cases of the C3 CRS

	Base Case		Optimal Case	
Compressor	Level m	$W_{m',m}$ (kW)	Level m	$W_{m',m}$ (kW)
C-1	2	2393.95	4	4809.61
C-2	4	2544.48	6	2183.09
C-3	6	1982.35	7	763.81
C-4	8	3668.96	8	986.93
TotW		10,589.74		8743.44

Table 5. Stream Information of the Optimal C3 CRS

m	m'	$fsc_{m,m'}$ (t/h)	$fb_{m,m'}$ (t/h)
0	4	279.76	–
4	6	–	167.32
6	7	–	110.65
7	8	–	89.09

Table 6. Distribution of Refrigerant Flow Rates and Cooling Duties in Each Evaporation Section of the Optimal C3 CRS

m	fg_m (t/h)	fe_m (t/h)	Qx_m (GJ/h)
0	–	279.76	–
4	112.44	167.32	41.23
6	56.67	110.65	13.74
7	21.56	89.09	6.20
8	89.09	–	37.92

Table 7. Minimum Utility Cost Comparison Between the Base and Optimal Cases of the C3 CRS[38]

	Base Case HEN	Optimal Case HEN
Overall cost ($/s)	66.40	1.73

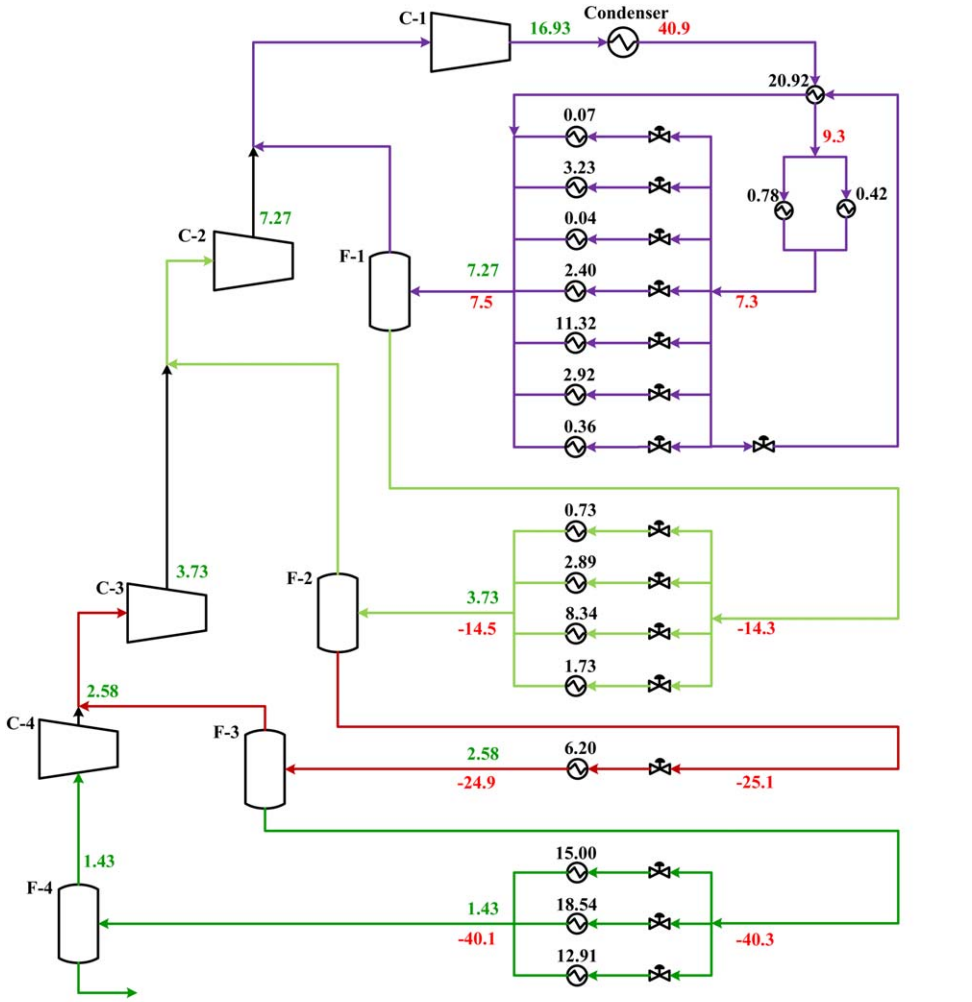

Figure 11. Design of the studied C3 CRS from the optimal solution.

[Color figure can be viewed in the online issue, which is available at wileyonlinelibrary.com.]

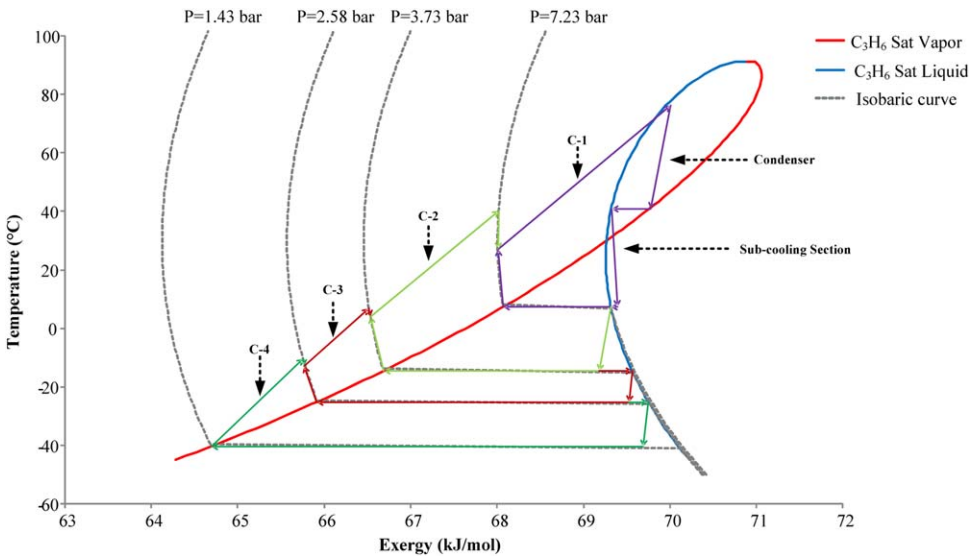

Figure 12. *B–T* plot of the optimized system.

[Color figure can be viewed in the online issue, which is available at wileyonlinelibrary.com.]

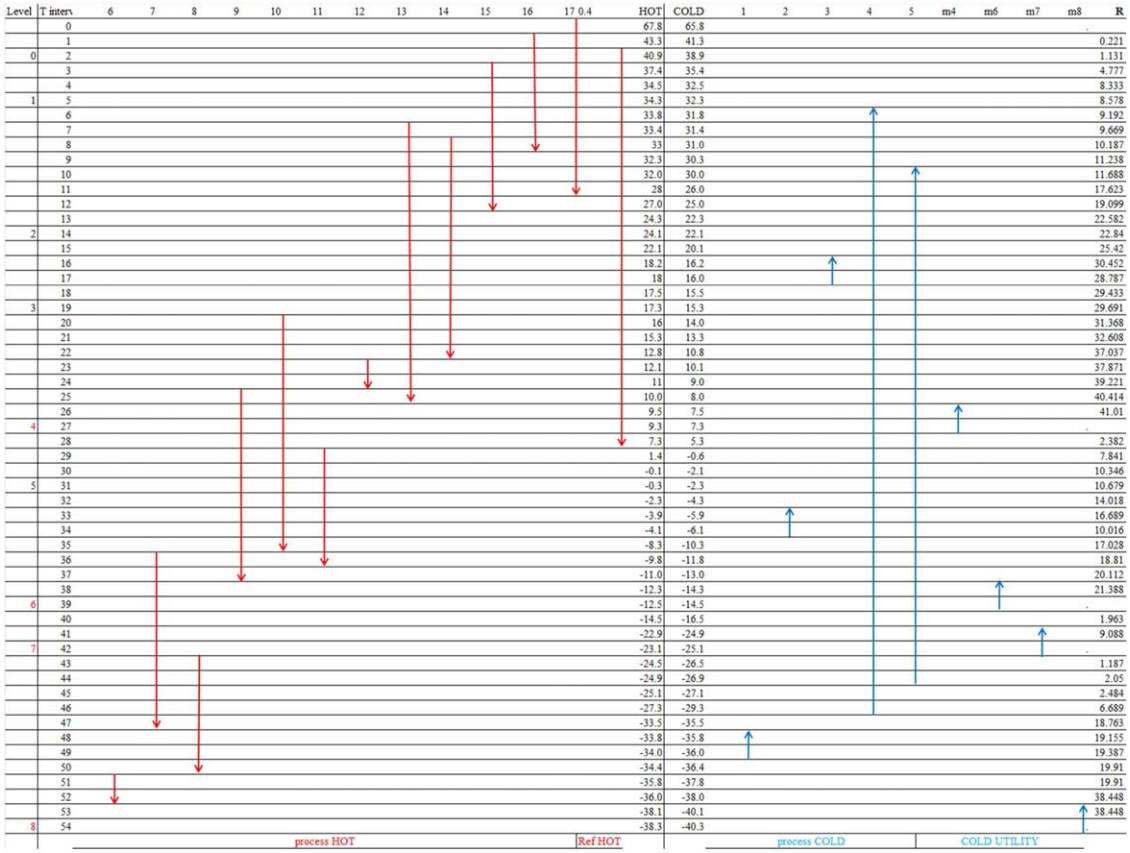

Figure 13. Heat distribution across temperature intervals of the C3 CRS.

[Color figure can be viewed in the online issue, which is available at wileyonlinelibrary.com.]

a significant refrigerant flow rate is distributed as well as the highest cooling demand is compromised ($Qx_4 = 41.23$ GJ/h, Table 6). Thus, the fourth level in the optimization case is more favorable comparing to the eighth level in the base case in terms of satisfying process cooling demands. According to the result shown in Table 5, an interlevel subcooling section exists in the resulted optimal solution, leaving the condenser outlet at the zeroth level (at 16.93 bar) and entering its consecutive level (at the fourth candidate pressure of 7.27 bar); while bypass valves connect the other following intermediate pressure levels. The minimum utility cost of both the base case and the optimal case are determined by a software developed by Taylor and Manousiouthakis based on the aforementioned work from Holiastos and Manousiouthakis.[22,38] The refrigerant, propylene in this case study, is priced at \$0.869/kg and the electricity cost for the compressor work remains as default at \$0.0025/kJ.[39] The minimum approach temperature is 2°C and the heat integration mode is selected as "heat exchanger network with heat pump network" using both hot and cold utilities. This establishes a lower bound to the refrigeration system without committing to a specific network structure.

Based on the optimal CRS and HEN synthesis, a new design of the studied C3 CRS from the optimal solution has been obtained, which is presented in Figure 11. After this optimization result from the MILP model is obtained, rigorous simulation with PR-BM property package is performed in Aspen Plus to validate its thermodynamic feasibility and consistency and to further refine our final solution.[40] Correspondingly, its *B*–*T* plot of the optimization case shown in Figure 12 can be obtained from Figure 11. Comparing Figures 12 to 10, the subcooling line of the optimization case stays closer to the saturation liquid line and the two longest expansion lines are avoided, signifying higher COP. The embedded HEN of the optimal C3 CRS cycle involves 54 temperature intervals, constructed from all of process and

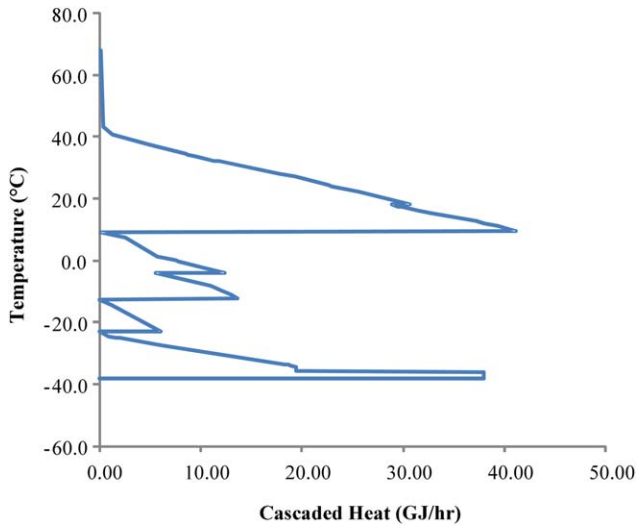

Figure 14. Grand composite curves of the optimal HEN synthesis.

[Color figure can be viewed in the online issue, which is available at wileyonlinelibrary.com.]

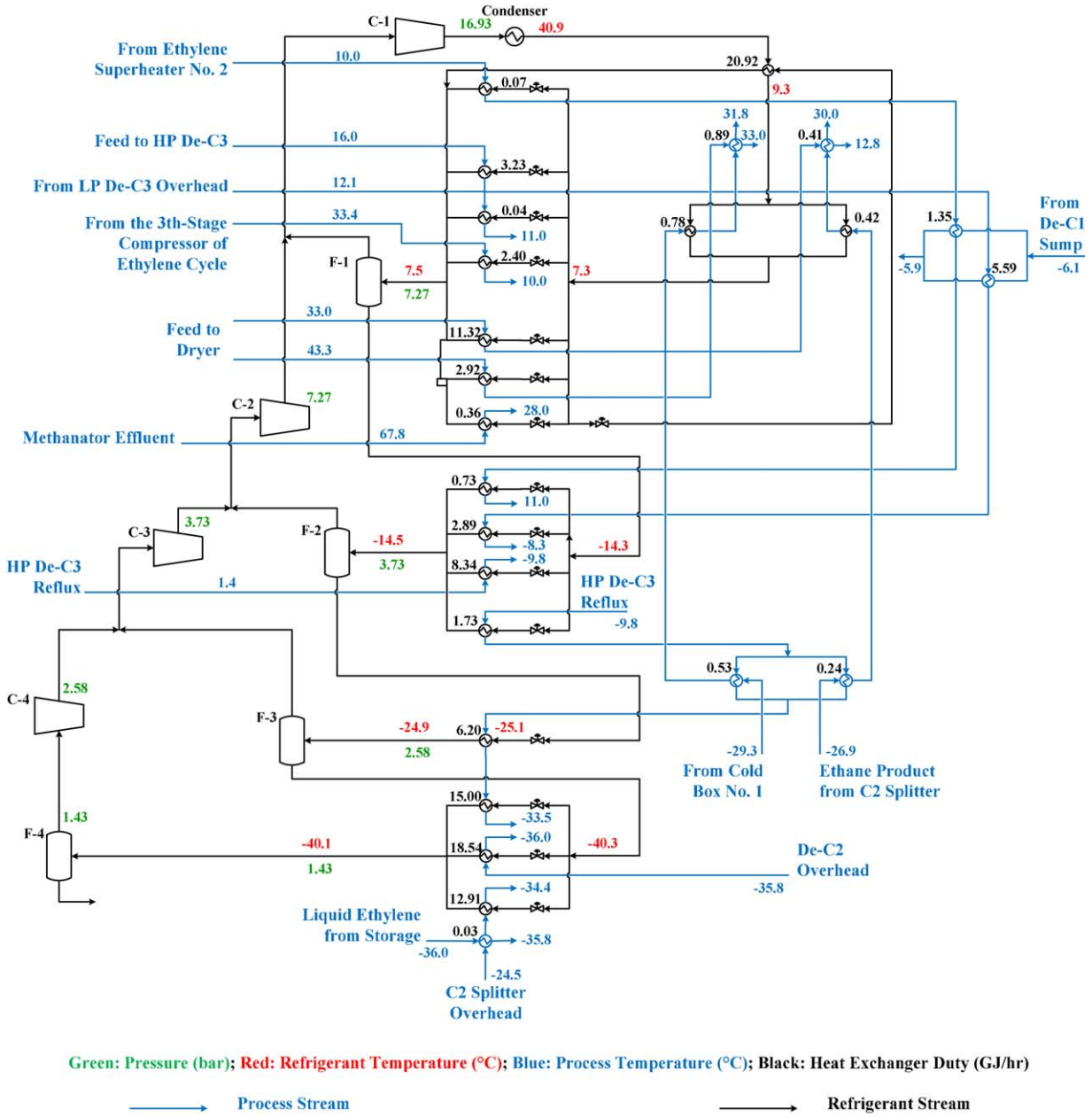

Figure 15. An optimal design of the C3 CRS integrated with a detailed HEN configuration.

[Color figure can be viewed in the online issue, which is available at wileyonlinelibrary.com.]

refrigerant inlet and outlet temperatures at various locations within the superstructure. It should be noted in Figure 13 that a propylene stream is considered as either hot streams if it passes through a subcooler or a cold stream if it passes through an evaporator. This figure also presents that the compression action at each level, which used work, is placed above its corresponding pinch point; hence, the optimal synthesis also agrees with Holiastos and Manousiouthakis's[22] conclusion (mentioned in the Introduction). Although the C3 CRS is a high-duty cycle, the grand composite curve in Figure 14 meets the vertical axis at both ends, indicating the resulted C3 CRS synthesis satisfies all of the process demands without the need for any additional utilities. This curve also presents the existence of three pinch points, each of which is equivalent to the saturated temperature of an intermediate pressure level (when m = 4, 6, or 7). The grand composite curve suggests several opportunities to configure the HEN to satisfy heat integration between streams from the hot side and cold side, regardless whether they are process or refrigerant streams.

Based on a manually trial-and-error method and heuristics, one possible HEN configuration satisfying both the thermodynamic matching and heat load presented in Figure 14 is proposed in Figure 15. It gives an optimal design of the studied C3 CRS together with a detailed HEN configuration. This overall design has been further validated through rigorous steady-state simulations to confirm the optimal solution feasibility. The refrigeration cycle (C3 CRS) is presented in black while the process side is in blue. The HEN design has 25 heat exchangers in total; 18 of them belong to the C3 CRS (Figure 11). The heat duty of each unit is also presented in Figure 15, together with the inlet and target temperatures of the process streams. The subcooling section connecting the condenser (the zeroth) pressure level (at

16.93 bar) with its intermediate lower one (at 7.27 bar) includes one heat exchanger placed in series with two parallel exchangers. The first subcooler is simultaneously acting as one of the evaporators at the 7.27-bar pressure level. Its two subsequent parallel subcoolers are heaters for two different process streams. Besides exchanging heat among process stream, the HEN synthesis result also suggests using part of the cooling duty from the subcooling section to evaporate a portion of refrigerant at a lower-pressure level. In addition to subcoolers and evaporators of the C3 CRS, the resulted HEN also contains seven heat changers, in which the process streams directly exchange heat with each other. The HEN synthesis suggests a more feasible structure to exchange heat among process streams; thus, lessening the demanding loads to the CRS.

In summary, the optimized C3 CRS shows merits in saving both compressor work and improved refrigeration performance. The proposed methodology provides deep insights into the studied CRS, which is beneficial for not only retrofitting existing processes but also new designs. The appearance of subcooler decreases exergy loss in excessive cooling duty by redirecting it toward thermal sinks at another locations. The candidate levels for the optimization model can be chosen under a more process-oriented guidance. Because the case study is a retrofitting problem, the original four-stage compressor is better to be used without significant modifications. Although the number of levels is kept intact in this case study, it can be a manipulated variable in designing a new refrigeration system. Implementation of HEN into the optimization model provides better heat integration since more pairing options are allowed and the temperature window is widened.

Concluding Remarks

An effective design and heat integration of a refrigeration system contributes a great deal in enhancing energy implementation of the whole plant. This study introduces a general methodology for optimal process synthesis of any CRSs. It employs exergy analysis as a driving force to identify process improvement opportunities, while computational simulation serves as both the exploring and evaluating tools. Besides, a mathematical model is presented to minimize the total compressor shaft work of the HEN-considered CRS cycle, where multiple refrigerants with multiple recycling loops satisfying all of cooling/heating demands are simultaneously addressed. Finally, the optimal solution is examined by rigorous simulations to verify its feasibility and consistency. The proposed methodology and mathematical model can not only help retrofitting an existing CRS but also designing new ones.

Acknowledgments

This work was supported in part by Texas Air Research Center and Graduate Student Scholarship from Lamar University.

Notations

Sets

$PH = \{n|1,\ldots,N\}$ = set of total number of hot process flows
$PC = \{l|1,\ldots,L\}$ = set of total number of cold process flows
$SJ = \{j|0,\ldots,J\}$ = set of temperature intervals in the heat-exchanger network
$SM = \{m|0,.,M\}$ = set of candidate levels

Parameters

C_p = average heat capacity of the refrigerant
Δhr_m = specific heat of vaporization at level m
Pm = candidate pressure at level m
T_m = refrigerant temperature at level m
$vf_{m'',m}$ = vapor fraction of bypassed valve from level m'' to level m
$wf_{m',m}$ = specific compressor shaft work from level m' to level m

Variables

f_0 = flow rate at condenser as total from the lower-pressure levels to the zeroth level
$fb_{m,m'}$ = bypassed flow rate if there is no subcooler from level m to level m'
$fc_{m',m}$ = inlet flow rate of compressor from level m' to level m
fe_m = liquid outlet flow rate from flash drum at level m
fg_m = vapor outlet flow rate from flash drum at level m
$fsc_{m,m'}$ = flow rate at the subcooler from level m to level m'
fv_m = vapor flow rate after bypass valve into level k
fx_m = inlet flow rate to flash drum at level m
fve_m = flow rate of vapor generated from evaporator at level m
Qx_m = exchanged heat in evaporator at level m
R_j = exiting residue heat between two consecutive temperature intervals at interval j
$W_{m',m}$ = compressor shaft work from level m' to level m
TotW = total compressor shaft work consumed by the system
ym = binary variable, which is 1 if pressure level m exists; otherwise, it is 0

Vectors

$xi_{j,m}$ = indicating binary heat index of refrigerant at level m in interval j
$Qp_{j,l}$ = partitioned heating demand of the cold process stream l within interval j
$Qp_{j,n}$ = partitioned cooling demand of the hot process stream n within interval j
$Qsc_{j,m'',m}$ = dimensionless heat fraction of refrigerant in subcooler from level m'' to level m within interval j

Literature Cited

1. Smith JM, Van Ness HC, Abbott MM. *Introduction to Chemical Engineering Thermodynamics, 7th ed*. New York, NY: McGraw-Hill, 2005:318–321.
2. Barnés FJ, King CJ. Synthesis of cascade refrigeration and liquefaction systems. *Ind Eng Chem Process Des Dev*. 1974;13:421–433.
3. Cheng WB, Mah RSH. Interactive synthesis of cascade refrigeration systems. *Ind Eng Chem Process Des Dev*. 1980;19:410–420.
4. Townsend WD, Linnhoff B. Heat and power networks in process design I: criteria for placement of heat engines and heat pumps in process networks. *AIChE J*. 1983;29:742–748.
5. Shelton MR, Grossmann IE. A shortcut procedure for refrigeration systems. *Comput Chem Eng*. 1985;9(6):615–619.
6. Shelton MR, Grossmann IE. Optimal synthesis of integrated refrigeration systems I. *Comput Chem Eng*. 1986;10:445.
7. Colmenares TR, Seider WD. Synthesis of cascade refrigeration systems integrated with chemical processes. *Comput Chem Eng*. 1989; 13(3):247–258.
8. Raman R, Grossmann IE. Relation between MILP modeling and logical inference for chemical process synthesis. *Comput Chem Eng*. 1991;15(2):73–84.
9. Raman R, Grossmann IE. Integration of logic and heuristic knowledge in MINLP optimization for process synthesis. *Comput Chem Eng*. 1992;16(3):155–171.
10. Vaidyaraman S, Maranas CD. Optimal synthesis of refrigeration cycles and selection of refrigerants. *AIChE J*. 1999;45:997–1017.
11. Wu G, Zhu XX. Retrofit of integrated refrigeration systems. *Trans IChemE*. 2001;79(A):163–181.
12. Zhang J, Xu Q. Cascade refrigeration system synthesis based on exergy analysis. *Comput Chem Eng*. 2011;35(9):1901–1914.

13. Zhang J, Wen YQ, Xu Q. Multi-objective optimization for design and operation of the chilling train system in ethylene plants. *Ind Eng Chem Res*. 2010;49:5786–5799.
14. Wilson S, Manousiouthakis V. IDEAS approach to process network synthesis: application to multicomponent MEN. *AIChE J*. 2000;46 (12):2408–2416.
15. Pena-Lopez J. *Synthesis of Energetically Efficient and Environmentally Friendly Process Flowsheets*. PhD Dissetation, University of California, Los Angeles, CA, 2012.
16. Grossmann IE, Yeomans H, Kravanja Z. A rigorous disjunctive optimization model for simultaneous flowsheet optimization and heat integration. *Comput Chem Eng*. 1998;22(Suppl.):S157–S164.
17. Duran MA, Grossmann IE. Simultaneous optimization and heat integration of chemical processes. *AIChE J*. 1986;32:123.
18. Quesada I, Grossmann IE. Global optimization of bilinear procass networks with multicomponent flows. *Comput Chem Eng*. 1995;19: 1219–1242.
19. Adjiman CS, Androulakis IP, Floudas CA. Global optimization of MINLP problems in process synthesis and design. *Comput Chem Eng*. 1997;21:445–450.
20. Zamora JM. Grossmann IE. A global MINLP optimization algorithm for the synthesis of heat exchanger networks with no stream splits. *Comput Chem Eng*. 1998;22:367–384.
21. Tawarmalani M, Sahinidis NV. A polyhedral branch-and-cut approach to global optimization. *Math Program*. 2005;103(2):225–249.
22. Holiastos K, Manousiouthakis V. Minimum hot/cold/electric utility cost for heat exchanger networks. *Comput Chem Eng*. 2002;26(1):3–16.
23. Yee TF, Grossmann IE. Simultaneous optimization models for heat integration—II. Heat Exchanger network synthesis. *Comput Chem Eng*. 1990;14:1165.
24. Linnhoff B, Hindmarsh E. The pinch design method for heat exchanger networks. *Chem Eng. Sci*. 1983;38(5):745–763.
25. Furman KC, Sahinidis NV. Computational complexity of heat exchanger network synthesis. *Comput Chem Eng*. 2001;25:1371–1390.
26. Furman KC, Sahinidis NV. A critical review and annotated bibliography for heat exchanger network synthesis in the 20th century. *Ind Eng Chem Res*. 2002;41:2335–2370.
27. Barbaro A, Bagajewicz MJ. New rigorous one-step MILP formulation for heat exchanger network synthesis. *Comput Chem Eng*. 2005; 29:1945–1976.
28. Wechsung A, Aspelund A, Gundersen T, Barton, PI. Synthesis of heat exchanger networks at subambient conditions with compression and expansion of process streams. *AIChE J*. 2011;57(8):2090–2108.
29. Cengel YA, Boles MA. *Thermodynamics An Engineering Approach, 5th ed*. New York, NY: McGraw-Hill Higher Education, 2005:423–470.
30. Aspelund A, Berstad DO, Gundersen T. An extended pinch analysis and design procedure utilizing pressure based exergy for subambient cooling. *Appl Thermal Eng*. 2007;27:2633–2649.
31. Peng DY, Robinson DB. A new two-constant equation-of-state. *Ind Eng Chem Fundam*. 1976;15:59–64.
32. Boston JF, Mathias, PM. *Phase Equilibria in a Third-Generation Process Simulator*. In: Proceedings of the 2nd International Conference on Phase Equilibria and Fluid Properties in the Chemical Process Industries. West Berlin, March 17–21, 1980:823–849.
33. Papoulias SA, Grossmann IE. A structural optimization approach to process synthesis—II. *Heat recovery network. Comput Chem Eng*. 1983;7:707–721.
34. GAMS, GAMS Development Corp.: Washington, DC, 2009.
35. Lee GC. Optimal design and analysis of refrigeration systems for low-temperature processes. PhD Dissetation, UMIST, UK, 2001.
36. McCain WD Jr. *Properties of Petroleum Fluids*, 2nd ed. PennWell: Tulsa, OK, 1990. Available at: http://www.knovel.com/web/portal/browse/display?_EXT_KNOVEL_DISPLAY_bookid=3615&VerticalID=0\. Accessed on March 17, 2013.
37. Tawarmalani M, Sahinidis NV. A polyhedral branch-and-cut approach to global optimization. *Math Program*. 2005;103(2):225–249.
38. Taylor LA, Manousiouthakis V. *Heat and Power Integration Program—Forms*. Copyright (c) 2002–2005, University of California and the program authors. From a project by Konstantinos Holiastos and Vasilios Manousiouthakis. Department Software and Computer Services, UCLA Engineering, Chemical and Biomolecular Engineering. Available at: http://www.chemeng.ucla.edu/resources/department-software-and-computer-services. Accessed on March 10, 2015.
39. Platts McGraw Hill Financial. Platts Global Petrochemical Index, 2014. Available at: http://www.platts.com/news-feature/2014/petrochemicals/pgpi/propylene. Accessed on March 10, 2015.
40. AspenTech, Inc. Aspen Physical Property System—Physical Property Methods, version 7.3: Aspen Technology, Inc.: Cambridge, MA, 2012.

Manuscript received Sep. 15, 2014, and revision received Mar. 13, 2015.